ARL-TN-0985 ● Dec 2019

DEVCOM ARMY RESEARCH LABORATORY

Investigation of Slip Kinematics in an Ultra-High Molecular Weight Polyethylene (UHMWPE) Laminar Composite Model

by Richard Becker

NOTICES

Disclaimers

The findings in this report are not to be construed as an official Department of the Army position unless so designated by other authorized documents.

Citation of manufacturer's or trade names does not constitute an official endorsement or approval of the use thereof.

Destroy this report when it is no longer needed. Do not return it to the originator.

ARL-TN-0985 ● DEC 2019

Investigation of Slip Kinematics in an Ultra-High Molecular Weight Polyethylene (UHMWPE) Laminar Composite Model

Richard Becker
Weapons and Materials Research Directorate, CCDC Army Research Laboratory

REPORT DOCUMENTATION PAGE

Form Approved
OMB No. 0704-0188

1. REPORT DATE *(DD-MM-YYYY)*	2. REPORT TYPE	3. DATES COVERED (From - To)
December 2019	Technical Note	August–October 2019

4. TITLE AND SUBTITLE
Investigation of Slip Kinematics in an Ultra-High Molecular Weight Polyethylene (UHMWPE) Laminar Composite Model

5a. CONTRACT NUMBER

5b. GRANT NUMBER

5c. PROGRAM ELEMENT NUMBER

6. AUTHOR(S)
Richard Becker

5d. PROJECT NUMBER

5e. TASK NUMBER

5f. WORK UNIT NUMBER

7. PERFORMING ORGANIZATION NAME(S) AND ADDRESS(ES)
CCDC Army Research Laboratory
ATTN: FCDD-RLW-B
Aberdeen Proving Ground, MD 21005

8. PERFORMING ORGANIZATION REPORT NUMBER
ARL-TN-0985

9. SPONSORING/MONITORING AGENCY NAME(S) AND ADDRESS(ES)

10. SPONSOR/MONITOR'S ACRONYM(S)

11. SPONSOR/MONITOR'S REPORT NUMBER(S)

12. DISTRIBUTION/AVAILABILITY STATEMENT
Approved for public release; distribution is unlimited.

13. SUPPLEMENTARY NOTES
ORCID ID(s): Richard Becker, 0000-0003-0104-856X; Web of Science Researcher ID I-1196-2013

14. ABSTRACT
Inclusion of explicit slip kinematics in a model for ultra-high molecular weight polyethylene fiber composites is investigated as a means of accommodating finite slip between the composite lamina with the goal of more efficient computations than explicitly depicting multiple slide surfaces through the thickness of a panel. The approach assumes finite shear in the plane of the fiber with plastic spin to accommodate the relative rotation. The stress is the sum of contributions from the fibers and the matrix material, with the enhanced kinematic description encompassed by the matrix. Results from preliminary simulations show that, while the model represents slip as intended, there is undesirable coupling among the different element layers that can be sufficiently severe to cause premature fiber failure. Simulations with multiple explicit slide surfaces have substantially more degrees of freedom, and they do not experience this adverse coupling. It is concluded that including slip kinematics in the composite constitutive relations is a viable approach for reducing the computational burden of the simulations prior to fracture but not beyond.

15. SUBJECT TERMS
ultra-high molecular weight polyethylene, UHMWPE, composite model, slip, polyethylene, slide surface

16. SECURITY CLASSIFICATION OF:			17. LIMITATION OF ABSTRACT	18. NUMBER OF PAGES	19a. NAME OF RESPONSIBLE PERSON
a. REPORT	b. ABSTRACT	c. THIS PAGE			Richard Becker
Unclassified	Unclassified	Unclassified	UU	24	19b. TELEPHONE NUMBER (Include area code) (410) 278-7980

Standard Form 298 (Rev. 8/98)
Prescribed by ANSI Std. Z39.18

Contents

List of Figures

List of Tables

1. Introduction

Ultra-high molecular weight polyethylene (UHMWPE) laminar composites used in ballistic applications typically deform with significant shear between the plies and extensive delamination. Successful finite element simulations[1] of the deformation, delamination, and perforation of the composites have been achieved using a fiber composite model in conjunction with slide surfaces separating each layer of elements in the composites. The bonding of the element layers is modeled with cohesive elements and associated constitutive relations. The slide surfaces account for the interlaminar slip to accommodate bending, and the slides also facilitate modeling separation of the layers. As the fibers are significantly damaged by the penetrator and fractured, the elements are eroded. To keep the solution tractable, each element layer represents several layers of oriented UHMWPE fibers. However, the number of element layers has to be sufficiently high to capture the bending and the penetration.

Simulating the UHMWPE composite with slides is effective,[2] but it is computationally very expensive. The increase in time over a simulation with a monolithic material was nearly a factor of 10 in initial simulations with EPIC.[3] The time increase has many sources. The number of finite element nodes in the target is roughly doubled, and the number of sliding contact constraints introduced is approximately equal to the number of target elements. Sliding and cohesive contact constraint equations must be solved at each contact segment, and these are solved twice in the robust double-pass algorithms. In addition, for multiprocessor simulations, the quantity of information communicated to adjacent processors increases significantly as data further from the domain boundaries are needed, and the slide surfaces must be repartitioned frequently among the processors as sliding and separation occur.

The significant cost of using explicit slide interfaces is acceptable if a limited number of simulations are to be run, but for design optimization studies, where hundreds or thousands of simulations are possible, a less costly option would be a substantial benefit. The intent of this work is to explore the use of a simple, special-purpose composite model that properly accounts for large-scale interlamina sliding as a less expensive alternative for situations where large deflections are expected, but with little penetration.

2. Laminar Model with Slip

The approach taken here is to represent explicitly the interlaminar slip in the deformation kinematics and to capture the stress as the sum of the fiber and the

matrix behavior. The kinematics, the stress increment, and the incremental solution algorithm are described in this section.

2.1 Notation

In the following, boldface Greek symbols and bold uppercase Latin letters represent second-rank tensors. Bold lowercase Latin letters represent vectors. Fourth-order tensors are given by double-struck, uppercase Latin symbols. Quantities with over-bars are effective quantities for the matrix, and dots over symbols denote a time rate. A dot between tensors implies an inner product, and a colon between second-rank tensors represents a contraction. The composition of a second-rank tensor from two vectors is indicated by the $\otimes$ symbol. The second-order identity is represented by $\boldsymbol{I}$.

2.2 Kinematics

The approach taken here is to represent the interlaminar slip explicitly in the deformation kinematics. The velocity gradient is decomposed additively into elastic and inelastic parts, $\boldsymbol{L} = \boldsymbol{L}_e + \boldsymbol{L}_{in-s} + \boldsymbol{L}_{in-p}$. Here, the inelastic part has been further decomposed into a slip, $\boldsymbol{L}_{in-s}$, and a more general plastic part, $\boldsymbol{L}_{in-p}$. The portion of the inelastic velocity gradient due to slip is expressed as

$$\boldsymbol{L}_{in-s} = \dot{\gamma}\,(\boldsymbol{s} \otimes \boldsymbol{m}), \tag{1}$$

where $\boldsymbol{s}$ is the slip direction and $\boldsymbol{m}$ is the slip plane normal. The shearing rate is $\dot{\gamma}$. The local slip plane is taken to be the plane formed by the two orthogonal UHMWPE fiber families. The normal is determined by the cross-product of the fiber family directions, $\boldsymbol{d}_1$ and $\boldsymbol{d}_2$ as $= \boldsymbol{d}_1 \times \boldsymbol{d}_2$. The slip direction, $\boldsymbol{s}$, is orthogonal to the slip plane normal, and the assumed direction is in the direction of the shear stress on the plane formed by the fibers.

The velocity gradient, and its elastic and plastic parts, can be represented as the sum of symmetric and antisymmetric parts, $\boldsymbol{L} = \boldsymbol{D} + \boldsymbol{\omega}$. The symmetric part, $\boldsymbol{D}$, is the rate of deformation tensor, and the antisymmetric part is the spin, $\boldsymbol{\omega}$.

The inelastic part of the rate of deformation tensor is patterned after J2 Flow Theory plasticity with an added slip component motivated by crystal plasticity models. It is given by

$$\boldsymbol{D}_{in-p} + \boldsymbol{D}_{in-s} = \dot{\bar{\varepsilon}}_m \frac{3}{2} \frac{\boldsymbol{\sigma}'_m}{\bar{\sigma}_m} + \dot{\gamma}\,\boldsymbol{P}\,. \tag{2}$$

The subscript m refers to the matrix material. $\dot{\bar{\varepsilon}}_m$ is an effective inelastic strain rate, $\boldsymbol{\sigma}'_m = \boldsymbol{\sigma}_m - \frac{1}{3}\boldsymbol{I}\,(\boldsymbol{\sigma}_m : \boldsymbol{I})$ is the deviatoric part of the stress tensor, and $\bar{\sigma}_m$ is the von Mises effective stress of the matrix. In the last term, $\dot{\gamma}$ is the interlaminar shear rate and

$$\boldsymbol{P} = \frac{1}{2}\,(\boldsymbol{s} \otimes \boldsymbol{m} + \boldsymbol{m} \otimes \boldsymbol{s}) \tag{3}$$

is the symmetric slip tensor. The antisymmetric slip tensor is

$$\boldsymbol{W} = \frac{1}{2}\,(\boldsymbol{s} \otimes \boldsymbol{m} - \boldsymbol{m} \otimes \boldsymbol{s}). \tag{4}$$

2.3 Matrix Deviatoric Stress Rate

The stress is assumed to have additive contributions from the fiber and matrix, and the matrix response is decomposed into deviatoric and volumetric parts. The matrix stress is related to the elastic strain of the matrix material. Assuming an elastic strain energy function, ϕ, the second Piola–Kirchhoff (P-K) stress in the matrix, $\boldsymbol{T}$, is related to the elastic Lagrangian strain, $\boldsymbol{E}_e$, by

$$\boldsymbol{T} = \frac{\partial\,\phi}{\partial\,\boldsymbol{E}_e}. \tag{5}$$

The relation between the second P-K stress and the Cauchy stress, $\boldsymbol{\sigma}$, is

$$\boldsymbol{\sigma}_m = J^{-1}\boldsymbol{F}_e \cdot \boldsymbol{T} \cdot \boldsymbol{F}_e^T\,, \tag{6}$$

where $\boldsymbol{F}_e$ is the elastic part of the deformation gradient from a multiplicative decomposition, $\boldsymbol{F} = \boldsymbol{F}_e \cdot \boldsymbol{F}_p$, and J is the determinant of $\boldsymbol{F}$. Taking the time derivative of the Cauchy stress

$$\begin{aligned}\dot{\boldsymbol{\sigma}}_m &= -\dot{J}\,J^{-1}\boldsymbol{\sigma}_m + \dot{\boldsymbol{F}}_e \cdot \boldsymbol{T} \cdot \boldsymbol{F}_e^T + \boldsymbol{F}_e \cdot \boldsymbol{T} \cdot \dot{\boldsymbol{F}}_e^T + \boldsymbol{F}_e \cdot \dot{\boldsymbol{T}} \cdot \boldsymbol{F}_e^T \\ &= -\dot{J}\,J^{-1}\boldsymbol{\sigma}_m + \dot{\boldsymbol{F}}_e \cdot \boldsymbol{F}_e^{-1} \cdot \boldsymbol{\sigma}_m + \boldsymbol{\sigma}_m \cdot \boldsymbol{F}_e^{-T} \cdot \dot{\boldsymbol{F}}_e^T + \boldsymbol{F}_e \cdot \left(\frac{\partial^2\phi}{\partial\,\boldsymbol{E}_e^2} : \dot{\boldsymbol{E}}_e\right) \cdot \boldsymbol{F}_e^T, \\ &= -\dot{J}\,J^{-1}\boldsymbol{\sigma}_m + \boldsymbol{L}_e \cdot \boldsymbol{\sigma}_m + \boldsymbol{\sigma}_m \cdot \boldsymbol{L}_e^T + \mathbb{C} :\, \dot{\boldsymbol{E}}_e\end{aligned} \tag{7}$$

$\mathbb{C}$ is the fourth-order modulus tensor. The velocity gradient can also be expressed as the sum of the rate of deformation tensor, $\boldsymbol{D}$, and the spin tensor, $\boldsymbol{\omega}$. In addition, the Lagrangian strain rate can be expressed in terms of the rate of deformation tensor as

$$\dot{\boldsymbol{E}} = \boldsymbol{F}^T \cdot \dot{\boldsymbol{D}} \cdot \boldsymbol{F} \tag{8}$$

so that the Cauchy stress rate of the matrix can be written as

$$\dot{\boldsymbol{\sigma}}_m = \boldsymbol{\omega}\cdot\boldsymbol{\sigma}_m - \boldsymbol{\sigma}_m\cdot\boldsymbol{\omega} + \mathbb{K}:\boldsymbol{D} - \mathbb{K}:\boldsymbol{D}_{in-p} \\ -[\mathbb{K}:\boldsymbol{D}_{in-s} + \boldsymbol{\omega}_{in-s}\cdot\boldsymbol{\sigma}_m - \boldsymbol{\sigma}_m\cdot\boldsymbol{\omega}_{in-s}] \quad . \tag{9}$$

The inelastic plastic spin is assumed to be zero. The fourth-order modulus $\mathbb{K}$ includes $\mathbb{C}$, several stress terms, and the volume change contribution. Substituting for the inelastic velocity gradient from Eqs. 1 and 2, the stress rate becomes

$$\dot{\boldsymbol{\sigma}}_m = \boldsymbol{\omega}\cdot\boldsymbol{\sigma}_m - \boldsymbol{\sigma}_m\cdot\boldsymbol{\omega} + \mathbb{K}:\boldsymbol{D} - \frac{3}{2}\frac{\dot{\bar{\varepsilon}}_m}{\bar{\sigma}_m}\,\mathbb{K}:\boldsymbol{\sigma}'_m \\ -\dot{\gamma}\,[\mathbb{K}:\boldsymbol{P} + \boldsymbol{W}\cdot\boldsymbol{\sigma}_m - \boldsymbol{\sigma}_m\cdot\boldsymbol{W}] \quad . \tag{10}$$

Assuming no coupling between the pressure and deviatoric response of the matrix, the stress is split into volumetric and deviatoric parts so that the pressure-volume response can be represented by a simplified equation of state for shock simulations. Further assuming that the matrix is isotropic, the modulus tensor can be replaced by a scalar shear modulus in Eq. 10, and the matrix deviatoric stress rate is

$$\dot{\boldsymbol{\sigma}}'_m = \boldsymbol{\omega}\cdot\boldsymbol{\sigma}'_m - \boldsymbol{\sigma}'_m\cdot\boldsymbol{\omega} + 2\mu\boldsymbol{D}' - 3\mu\dot{\bar{\varepsilon}}_m\frac{\boldsymbol{\sigma}'_m}{\bar{\sigma}_m} - \dot{\gamma}\boldsymbol{R}\,, \tag{11}$$

where

$$\boldsymbol{R} = 2\mu\boldsymbol{P} + \boldsymbol{W}\cdot\boldsymbol{\sigma}'_m - \boldsymbol{\sigma}'_m\cdot\boldsymbol{W}. \tag{12}$$

2.4 Matrix Stress Integration

The subscript *m* is dropped in this section for clarity. The stress is for the matrix only. Equation 11 is integrated over a time step Δt as

$$\boldsymbol{\sigma}'_{t+\Delta t} = \boldsymbol{\sigma}'_t + \Delta t(\boldsymbol{\omega}\cdot\boldsymbol{\sigma}'_t - \boldsymbol{\sigma}'_t\cdot\boldsymbol{\omega} + 2\mu\boldsymbol{D}') - 3\mu\dot{\bar{\varepsilon}}\Delta t\frac{\boldsymbol{\sigma}'_{t+\Delta t}}{\bar{\sigma}_{t+\Delta t}} - \dot{\gamma}\Delta t\boldsymbol{R}\,. \tag{13}$$

The first two terms are grouped together as the trial stress, $\boldsymbol{\sigma}^T$. This includes the incremental rotation from the material spin in addition to the strain increment. From Eq. 13, the plastic term is moved to the left-hand side to give

$$\boldsymbol{\sigma}_{t+\Delta t}(1 + 3\mu\dot{\bar{\varepsilon}}\Delta t/\bar{\sigma}_{t+\Delta t}) = \boldsymbol{\sigma}^T - \dot{\gamma}\Delta t\boldsymbol{R} = \boldsymbol{B}\,. \tag{14}$$

The stress at the end of the time step depends on the applied strain at a material point and relaxation due to either slip, plasticity, or both. The approach is to first determine if slip is active. If it is, is general plasticity also active? If slip is not active, is general plasticity active?

2.4.1 Slip Vector Calculation

Before the resolved shear stress on the slip plane can be determined, the direction of slip is needed for Eqs. 1 and 3. The resolved traction on the slip plane is the projection of the Cauchy stress tensor onto the plane normal. The direction of slip is assumed to be in the direction of the maximum shear traction. For isotropic slip in the plane, this will be in the direction of the projected trial stress, $\boldsymbol{t} = \boldsymbol{m} \cdot \boldsymbol{\sigma}^T$. The slip direction within the plane is found by subtracting the projection of the traction on the normal from the total traction,

$$\boldsymbol{s} = \frac{\boldsymbol{t} - \boldsymbol{m}(\boldsymbol{t} \cdot \boldsymbol{m})}{|\boldsymbol{t} - \boldsymbol{m}(\boldsymbol{t} \cdot \boldsymbol{m})|} . \tag{15}$$

2.4.2 Slip Only

Active slip is determined by setting $\dot{\bar{\varepsilon}}$ in Eq. 14 to zero and projecting the equation onto the slip tensor as

$$\boldsymbol{P}: \boldsymbol{\sigma}_{t+\Delta t} = \tau = \boldsymbol{P}: \boldsymbol{\sigma}^T - \dot{\gamma} \Delta t \boldsymbol{P}: \boldsymbol{R} . \tag{16}$$

The left-hand side of the equation is the resolved shear stress, τ. If the projected trial stress exceeds the critical resolved shear stress, $\boldsymbol{P}: \boldsymbol{\sigma}^T > \tau_c$, slip must occur to reduce the resolved shear stress to the critical value.

$$\dot{\gamma}\, \Delta t = \begin{cases} 0 & \text{if } \boldsymbol{P}: \boldsymbol{\sigma}^T \leq \tau_c \\ (\boldsymbol{P}: \boldsymbol{\sigma}^T - \tau_c)/(\boldsymbol{P}: \boldsymbol{R}) & \text{if } \boldsymbol{P}: \boldsymbol{\sigma}^T > \tau_c \end{cases} . \tag{17}$$

Once the slip rate is known, $\boldsymbol{B}$ is calculated from Eq. 14, and its effective scalar magnitude is determined by

$$\sqrt{\frac{3}{2} \boldsymbol{B}: \boldsymbol{B}} = \bar{B} . \tag{18}$$

If $\dot{\gamma} = 0$, general plasticity is evaluated through Section 2.4.3. If $\dot{\gamma} > 0$, general matrix plasticity is also possible. If $\bar{B} \leq \sigma_c$, the matrix flow stress, then there is no general plasticity, $\boldsymbol{\sigma}_{t+\Delta t} = \boldsymbol{B}$, and the solution for the time step is complete. If there is also general plasticity, the solution proceeds according to Section 2.4.4.

2.4.3 General Plasticity Only

If the slip rate is zero from Eq. 17, there is still the possibility of general plasticity. In this case, Eq. 14 is the standard J2–Flow Theory plasticity relation. Assuming a von Mises yield strength of σ_c, the plastic strain rate is determined from

$$\dot{\bar{\varepsilon}}\, \Delta t = \begin{cases} 0 & \text{if } \sigma_e^T \leq \sigma_c \\ (\sigma_e^T - \sigma_c)/3\mu & \text{if } \sigma_e^T > \sigma_c \end{cases} , \tag{19}$$

where the effective trial stress is defined as

$$\sigma_e^T = \sqrt{\frac{3}{2}\boldsymbol{\sigma}^T : \boldsymbol{\sigma}^T}\,. \tag{20}$$

The Cauchy stress is then calculated from the standard radial return method as

$$\boldsymbol{\sigma}_{t+\Delta t} = \begin{cases} \boldsymbol{\sigma}^T & \text{if } \sigma_e^T \le \sigma_c \\ \boldsymbol{\sigma}^T \sigma_c / \sigma_e^T & \text{if } \sigma_e^T > \sigma_c \end{cases}. \tag{21}$$

2.4.4 Slip and General Plastic Deformation

When both mechanisms are active, contracting Eq. 14 with itself, multiplying by 3/2, and taking the square root results in

$$\bar{\sigma}_{t+\Delta t}(1 + 3\mu\dot{\bar{\varepsilon}}\Delta t/\bar{\sigma}_{t+\Delta t}) = \sqrt{\frac{3}{2}\boldsymbol{B}:\boldsymbol{B}} = \bar{B}\,. \tag{22}$$

Dividing Eq. 14 by Eq. 22, and rearranging

$$\boldsymbol{\sigma}_{t+\Delta t}\bar{B} = \bar{\sigma}_{t+\Delta t}\boldsymbol{B} = \bar{\sigma}_{t+\Delta t}\,\boldsymbol{\sigma}^T - \bar{\sigma}_{t+\Delta t}\,\dot{\gamma}\Delta t\,\boldsymbol{R}\,. \tag{23}$$

Projecting Eq. 23 onto the slip tensor,

$$\boldsymbol{P}:\boldsymbol{\sigma}_{t+\Delta t}\bar{B} = \bar{\sigma}_{t+\Delta t}\,\boldsymbol{P}:\boldsymbol{\sigma}^T - \bar{\sigma}_{t+\Delta t}\,\dot{\gamma}\Delta t\,\boldsymbol{P}:\boldsymbol{R}\,. \tag{24}$$

The material is slipping in this case, so the projected shear stress will equal the critical resolved shear stress, $\boldsymbol{P}:\boldsymbol{\sigma}_{t+\Delta t} = \tau_c$. Since there is also general plastic deformation, $\bar{\sigma}_{t+\Delta t} = \sigma_c$.

Having eliminated the general plastic strain rate from Eq. 24 by the above division, everything in the relation is known except for the slip rate. The slip rate is also embedded in $\bar{B}$, so the solution is facilitated by squaring Eq. 24, resulting in

$$\begin{aligned} &\frac{3}{2}\,\tau_c^2\,[(\boldsymbol{\sigma}^T:\boldsymbol{\sigma}^T) - 2(\dot{\gamma}\Delta t)(\boldsymbol{\sigma}^T:\boldsymbol{R}) + (\dot{\gamma}\Delta t)^2(\boldsymbol{R}:\boldsymbol{R})] \\ &= \bar{\sigma}_{t+\Delta t}^2[(\boldsymbol{P}:\boldsymbol{\sigma}^T)^2 - 2(\dot{\gamma}\Delta t)(\boldsymbol{P}:\boldsymbol{\sigma}^T)(\boldsymbol{P}:\boldsymbol{R}) + (\dot{\gamma}\Delta t)^2(\boldsymbol{P}:\boldsymbol{R})^2 \end{aligned}. \tag{25}$$

The terms on the left largely result from $\bar{B}^2$. Rearranging the terms, Eq. 25 can be put in the form of a quadratic equation to solve for the slip rate.

$$\begin{aligned} (\dot{\gamma}\Delta t)^2\left[(\boldsymbol{P}:\boldsymbol{R})^2 - \frac{3}{2}\frac{\tau_c^2}{\sigma_y^2}(\boldsymbol{R}:\boldsymbol{R})\right] - 2(\dot{\gamma}\Delta t)\left[(\boldsymbol{P}:\boldsymbol{\sigma}^T)(\boldsymbol{P}:\boldsymbol{R}) - \frac{3}{2}\frac{\tau_c^2}{\sigma_y^2}(\boldsymbol{\sigma}^T:\boldsymbol{R})\right] \\ + \left[(\boldsymbol{P}:\boldsymbol{\sigma}^T)^2 - \frac{3}{2}\frac{\tau_c^2}{\sigma_y^2}\right] = 0 \end{aligned}. \tag{26}$$

Once the slip rate has been determined, it can be substituted into Eq. 22 to determine the strain rate $\dot{\bar{\varepsilon}}$ from

$$\dot{\bar{\varepsilon}}\,\Delta t = \frac{\bar{B} - \sigma_c}{3\mu}. \tag{27}$$

Then the matrix contribution to the Cauchy stress can be found using the first equality in Eq. 23, which is essentially a radial return in the direction of $\boldsymbol{B}$.

$$\boldsymbol{\sigma}_{t+\Delta t} = \boldsymbol{B}\,\frac{\bar{\sigma}_{t+\Delta t}}{\bar{B}}. \tag{28}$$

2.5 Matrix Equation of State

The equation of state (EOS) for the matrix material is assumed to follow the mechanical form of the Murnaghan EOS. Using the relative volume calculated from the determinant of the deformation gradient, J, the hydrostatic component of the matrix stress is determined by

$$\sigma_{m-h} = -\frac{\kappa}{\kappa'}\left[J^{-\kappa'} - 1\right], \tag{29}$$

where κ is the bulk modulus and κ' is the derivative of the bulk modulus with respect to pressure. Any temperature dependence is ignored for this simple model.

The total stress contribution for the matrix is the sum of the hydrostatic stress and the deviatoric part from Section 2.4.

2.6 Fiber Stress

Stress in the fiber families is assumed to be a function of the fiber stretch. Fiber directions in the undeformed configuration are specified by the model input as unit vectors $\boldsymbol{d}_{i0}$. The deformed vectors are calculated using the deformation gradient,

$$\boldsymbol{d}_i = \boldsymbol{F} \cdot \boldsymbol{d}_{i0}. \tag{30}$$

The stretch is determined as $\lambda_i = \sqrt{\boldsymbol{d}_i \cdot \boldsymbol{d}_i}$ (no summation on i), and the stress due to the fiber stretch is

$$\boldsymbol{\sigma}_{if} = \begin{cases} E\,(\lambda_i - 1)/[1 + A(1 - \lambda_i)] & \text{if } \lambda_i \le 1 \\ E\,(\lambda_i - 1) & \text{if } \lambda_i > 1 \end{cases}. \tag{31}$$

Here, E is the fiber modulus, and the form for the $\lambda_i < 1$ branch is chosen to limit the compressive stress and simulate buckling.[4] The compressive stress is linear in stretch near $\lambda_i = 1$ and smoothly asymptotes to E/A, where A is a softening parameter.

The fiber stress, the hydrostatic stress, and the matrix stress are added to give the total stress for the composite. The volume fraction weighting is not considered in this simple model, so the properties for the individual components should be weighted according to the volume fraction.

2.7 Fiber Damage

Fiber damage is assumed to accumulate with stretch to avoid fracture due to noise and to include a pressure dependence. Damage, $\mathcal{D}$, is integrated through time as

$$\mathcal{D}_{t+\Delta t} = \mathcal{D}_t + \frac{E\langle \lambda - \lambda_{max} \rangle}{\sigma_{ffail} - a\, \sigma_{m-h}}, \tag{32}$$

where λ_{max} is the maximum prior stretch attained by the fiber, and $\langle - \rangle$ are Macaulay brackets. Damage does not accumulate if the current stretch is less than this maximum, λ_{mas}. Otherwise, the damage variable is unchanged. The σ_{ffail} in Eq. 34 is the fiber failure stress, and σ_{m-h} is the hydrostatic stress in the matrix material.

The purpose of the hydrostatic stress term is to offset the addition of the pressure associated with stress normal to the composite. The magnitude of the normal stress due to impact can exceed the composite tensile failure strength, and this pressure generally does not initiate fiber failure. The parameter a in Eq. 32 is expected to be on the order of unity.

2.8 Implementation as an Abaqus/UMAT

The model described in the previous sections was implemented as an Abaqus/UMAT subroutine and it is run in EPIC for evaluation.

3. Model Evaluation

The model is evaluated in a simple plate impact configuration by comparing the solution with explicit slide surfaces to the solution using shear within the elements. The comparison presented is limited to the critical results that illustrate the limitations of the approach.

3.1 Impact Geometry and Material Properties

The model is evaluated in a configuration where a 12.7-mm-diameter, 4340 steel sphere impacts a 7.8-mm-thick panel at 293 m/s and normal incidence, as shown in Fig. 1a. The impactor is discretized with nine shells of elements across the radius and the panel is represented by 20 hexahedral elements through the thickness. The element aspect ratios are approximately 1:1 (Fig. 1b).

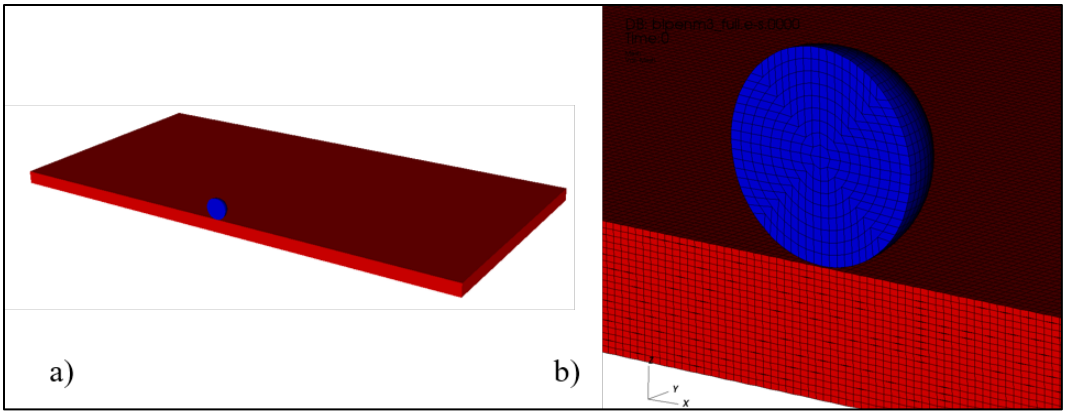

Fig. 1 Impact geometry: a) half-symmetry model and b) enlarged view showing the mesh

The two orthogonal fiber families lie in the plane of the target in the x and y directions.

The reference solution is one where cohesive elements and slide surfaces are placed between each element layer in the target. Thus, each layer of elements represents several cross-ply layers of UHMWPE fibers. The cohesive elements are given a strength of 6 MPa, a tangential separation length of 0.5 mm, and a normal separation length of 0.5 mm.

Except for the slip strength, τ_c, the same parameters are used for both the simulation with slide surfaces and without (Table 1). For the analysis with slide surfaces, the strength for slip is set high to prohibit slip, $\tau_c = 500$ MPa.

Table 1 Parameters used in the material model

ρ g/cm^3	μ GPa	κ GPa	κ'	σ_c MPa	τ_c MPa	E GPa	σ_{ff} GPa	A	a
0.987	1.0	2.0	8	150	5	52.8	1.5	10	1.5

3.2 Results Prior to Fracture

For an equivalent time prior to element failure, the simulation without the sliding surface between each element layer took 11 min on a single processor while the simulation with the sliding surfaces took 102 min. The code statistics show a bit over 16% of the time was spent in the slide algorithm for the former and over 85% for the latter.

The fiber stretch at the symmetry plane is plotted in Fig. 2 for the simulations with and without explicit slide surfaces at 6 μs of simulation time. There are two important observations from the comparison. First is that the stretch is similar for the two simulation methods. Detailed examination reveals that the stretch is

somewhat higher in the shear result than the slip, but the rough similarity suggests that the shear in the new formulation is performing much the same way as the discrete slip.

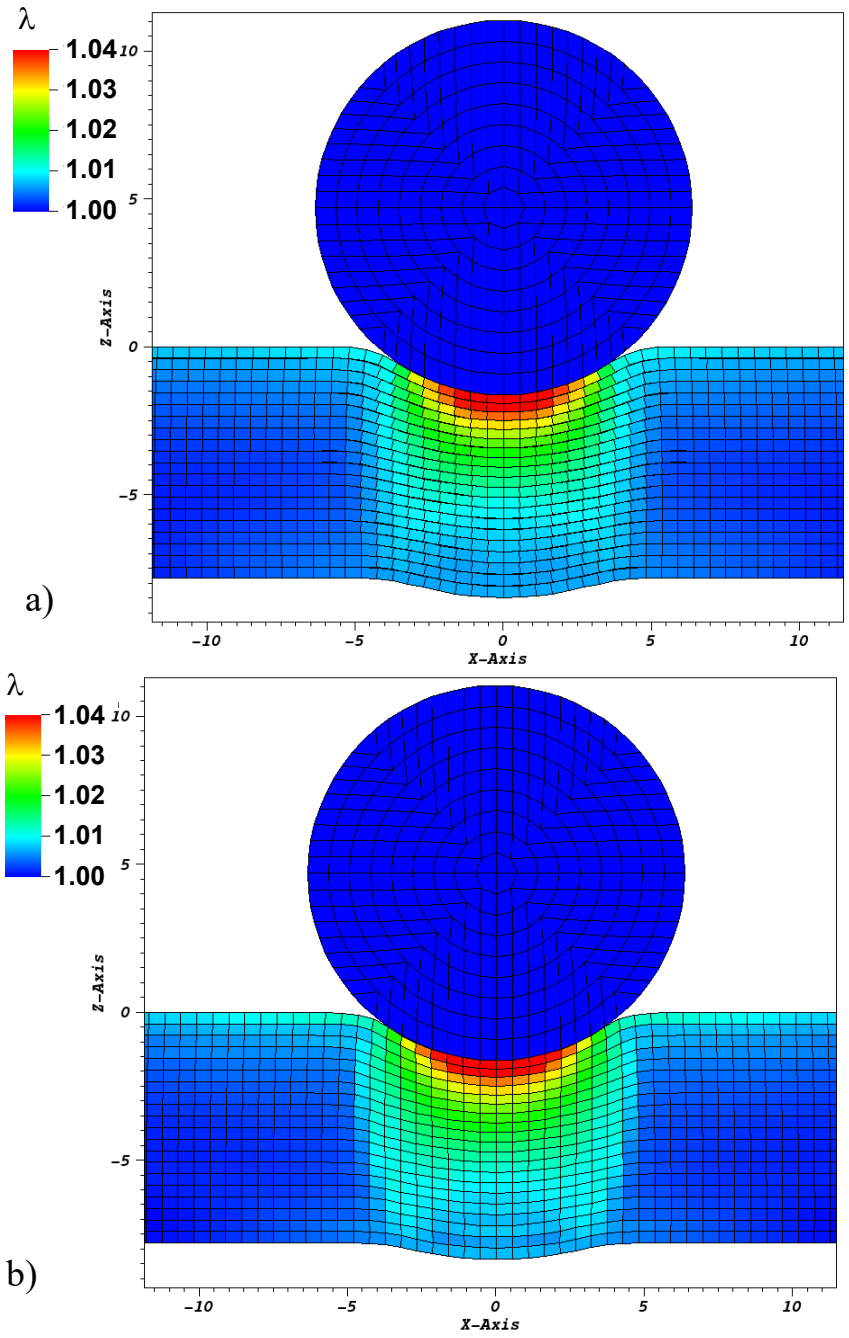

Fig. 2 In-plane fiber stretch at 6 μs for a) simulation with explicit slide surfaces and b) simulation with continuum slip

The second observation concerns the angle of the initially vertical element boundaries near the edge of the penetrator. In the simulation with the explicit slide surfaces, these boundaries show overall rotation with the element surfaces, whereas they remain more vertical for the continuum slip simulation. This shows the plastic spin needed to make the roughly inextensible fibers conform to the overall deformation. If the upper-left corners of the elements of successive layers in Fig. 2a were connected, they show a vertical alignment similar to the element sides of Fig. 2b. The sliding and rotation are captured by the shear model.

The longitudinal stress distribution is also similar for the two simulation techniques, as shown in Fig. 3. The stress is 20 MPa or so lower in the simulation with explicit slip, but the overall distribution and patterns are similar. The goal is not to have the results be identical, but for the sliding mechanism to be appropriately captured by the slip.

It is notable that the longitudinal stress is higher in the second layer of elements than the top layer. With the stress being significantly higher than the matrix flow strength, the longitudinal stress is essentially the sum of the negative matrix hydrostatic stress and the positive fiber stress. The magnitude of the hydrostatic stress is greater in the top layer than the second, which offsets the tensile stress.

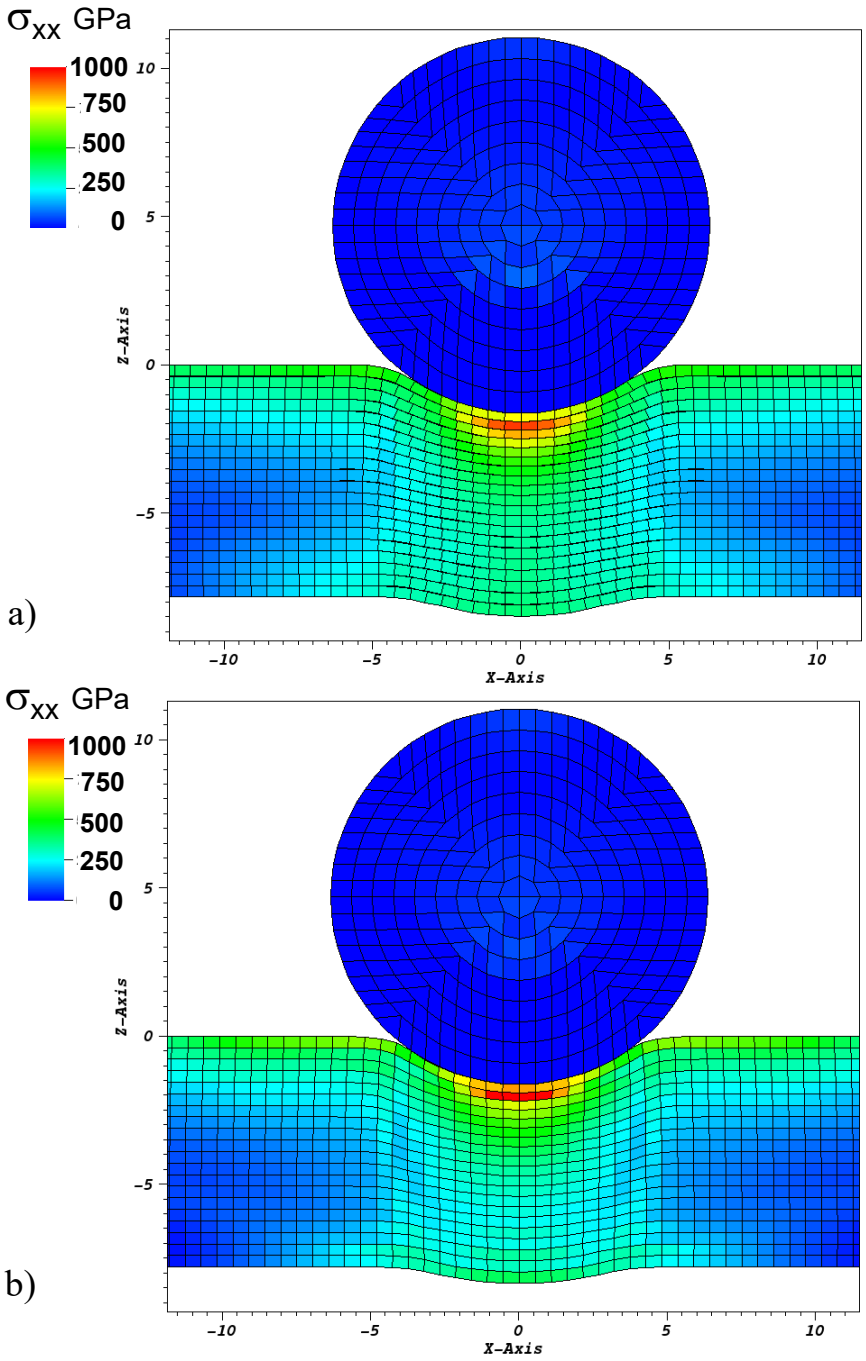

Fig. 3 Axial stress distribution at 6 μs for a) simulation with explicit slide surfaces and b) simulation with continuum slip

3.2 Fiber Failure Progression

Material failure due to fiber stretch is indicated by the red in Fig. 4 for the two simulations. Plots are obtained every 1 μs, and since the fiber is stretching a bit faster in the slip simulation, the plot is at 7 μs for the slip simulation and at 8 μs for the simulation with explicit slide surfaces.

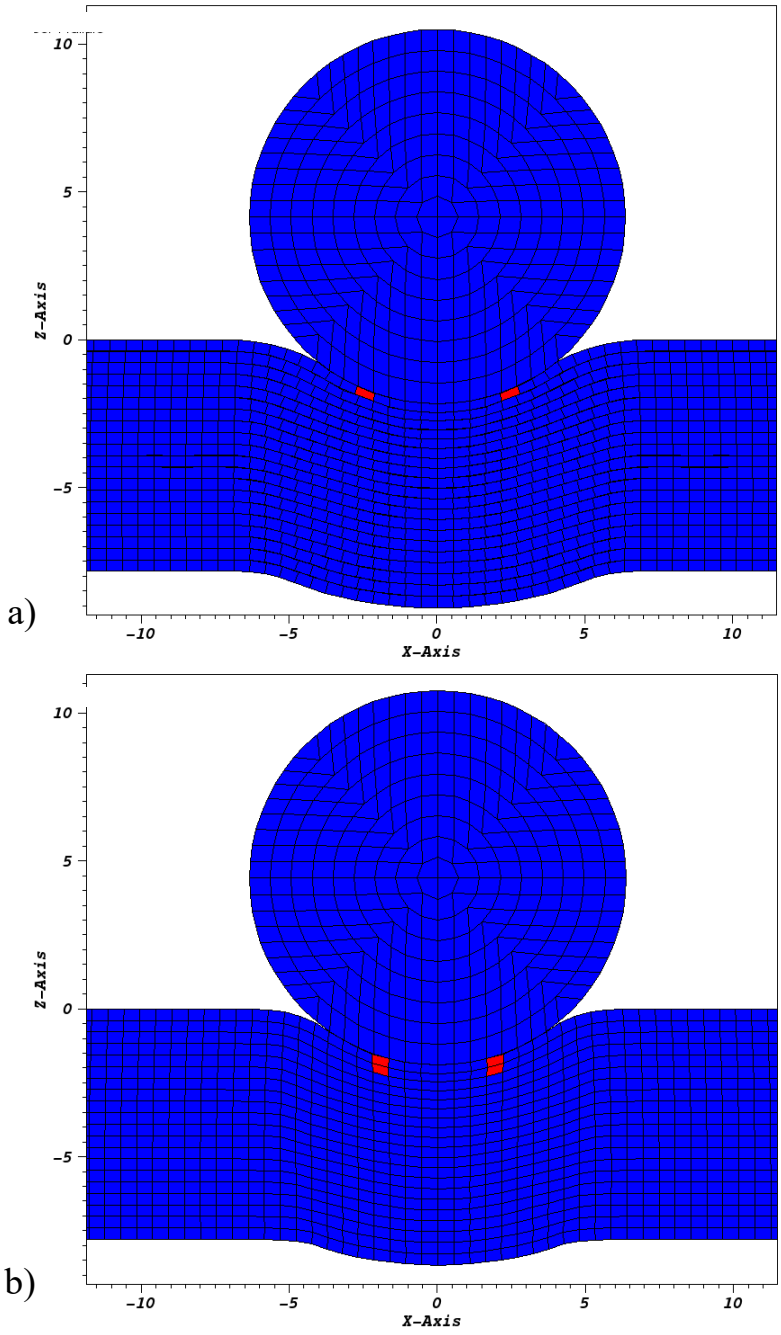

Fig. 4 Fiber failure is indicated in red: a) simulation with explicit slide surfaces at 8 μs and b) simulation with continuum slip at 7 μs

The important feature to note about the failure patterns is that the failure quickly propagates to the second row of elements in the simulation with continuum shear (Fig. 4b). There is significant tensile stress and elastic stretch in the fibers prior to fracture. When the fibers break, the extension load that had been sustained by the broken layer is partially transmitted to the layer below through the contiguous mesh. This quickly initiates failure in the second layer.

The discrete slides, on the other hand, offer greater isolation between the successive layers so that the stress concentration on the neighboring layer is substantially reduced. The fractured layer slips on the layer below, resulting in a more uniform stress redistribution.

Undesirable coupling between layers was observed in other regions of the simulation at other times. Some of these were more subtle. The couplings often involved something akin to an hourglass mode where a gradient produced hourglass-type patterns that affected the stretch and shear of underlying layers. The elements have constant shear, and steep gradients within the plane of the fibers would require finer resolution to be represented appropriately.

4. Conclusions

The introduction of shear explicitly into the kinematics of a composite model successfully captures the large in-plane shear associated with deformation of UHMWPE, cross-ply fiber composites. However, the continuous mesh provides a degree of coupling between layers that introduces nonphysical forces in the neighborhood of sharp gradients, such as fractures.

The simulation with explicit slide surfaces, on the other hand, has roughly two-thirds more degrees of freedom that accommodate in-plane relative motion between layers. These provide ample mobility to allow fiber failure without transmitting undue stress to adjacent layers.

This preliminary analysis suggests that the proposed model will not be useful for the intended application beyond initial fracture. Hence, there is no impetus to pursue the addition of delamination or other features into this framework. While the use of multiple explicit slide surfaces is more computationally expensive, the solution is far superior once fracture initiates. While the current developments are useful for large deformation, the use of multiple slide surfaces is the recommended approach for simulations involving fiber failure.

5. References

1. Zhang TG, Satapathy SS, Vargas-Gonzalez LR, Walsh SM. Effect of boundary conditions on the back face deformations of flat UHMWPE panels. Aberdeen Proving Ground (MD): Army Research Laboratory (US); 2014 Dec. Report No.: ARL-RP-0514.

2. Zhang TG, Satapathy SS, Vargas-Gonzalez LR, Walsh SM. Modeling ballistic response of ultra-high-molecular-weight polyethylene (UHMWPE). Aberdeen Proving Ground (MD): Army Research Laboratory (US); 2016 July. Report No.: ARL-TR-7723.

3. Johnson GR, Beissel SR, Gerlach CA, Holmquist TJ. User instruction for the 2018 version of EPIC. US Army Tank Automotive Research, Development and Engineering Center; 2018. Final Report. NAMC Agreement No. 69-201501, CVS OTA RPP10, Project SUR-17-06.

4. Love BM. CCDC Army Research Laboratory, Aberdeen Proving Ground, MD. Private communication, 2019 Apr.

List of Symbols, Abbreviations, and Acronyms

$\mathbb{C}$	Lagrangian modulus
$\boldsymbol{d}_i$	fiber direction
$\boldsymbol{D}$	rate of deformation tensor
$\boldsymbol{E}$	Green–Lagrange strain
$\boldsymbol{F}$	deformation gradient
$\boldsymbol{I}$	second-order identity tensor
J	determinant of the deformation gradient
$\mathbb{K}$	stress-modified modulus
$\boldsymbol{L}$	velocity gradient
$\boldsymbol{m}$	slip plane normal
$\boldsymbol{P}$	symmetric slip tensor
$\boldsymbol{R}$	projected modulus modified with rotated stress
$\boldsymbol{s}$	slip direction
$\boldsymbol{T}$	second Piola–Kirchhoff stress
$\boldsymbol{W}$	antisymmetric slip tensor
Δt	time increment
$\dot{\bar{\varepsilon}}$	effective plastic strain rate
$\dot{\gamma}$	shearing rate
ϕ	elastic strain energy function
μ	elastic shear modulus
$\boldsymbol{\sigma}$	Cauchy stress
$\bar{\sigma}$	von Mises effective stress
σ_c	critical flow stress of the matrix
σ_e^T	effective trial stress
$\boldsymbol{\sigma}T$	trial stress
τ_c	critical resolved shear stress of the matrix

ϕ	elastic strain energy function
$\boldsymbol{\omega}$	spin tensor
ARL	Army Research Laboratory
CCDC	US Army Combat Capabilities Development Command
EOC	equation of state
P-K	Piola–Kirchhoff
UHMWPE	ultra-high molecular weight polyethylene

1 (PDF) DEFENSE TECHNICAL INFORMATION CTR DTIC OCA

1 (PDF) CCDC ARL FCDD RLD CL TECH LIB

18 (PDF) CCDC ARL FCDD RLW B R C BECKER J CAMPBELL P GILLICH C HOPPEL B SCHUSTER A TONGE L VARGAS-GONZALEZ FCDD RLW PB T BAUMER T WEERASOORIYA S WOZNIAK T ZHANG FCDD RLW PE M LOVE FCDD RLW M B LOVE FCDD RLW MA T BOGETTI M YEAGER FCDD RLW MB D O'BRIEN FCDD RLW MC J SNYDER FCDD RLW MG J LENHART